BIOMICROFLUIDICS **10**, 054119 (2016)

Modulating wall shear stress gradient via equilateral triangular channel for *in situ* cellular adhesion assay

Hyung Woo Kim, Seonjin Han, Wonkyoung Kim, Jiwon Lim, and Dong Sung Kim[a)]
Department of Mechanical Engineering, Pohang University of Science and Technology (POSTECH), 77 Cheongam-ro, Nam-gu, Pohang 37673, South Korea

(Received 9 August 2016; accepted 8 October 2016; published online 17 October 2016)

This study introduces an equilateral triangular channel (ETRIC), a novel microfluidic channel with an equilateral triangular cross-section, for cell adhesion assay by modulating the wall shear stress (WSS) gradient. The channel can generate a parabolic WSS gradient perpendicular to the flow direction at a single flow rate, and cell detachment can be *in situ* screened in response to spatially different levels of WSS. The existence of a simple form of exact solution for the velocity field inside the entire ETRIC region enables the easy design and modulation of the WSS levels at the bottom surface; therefore, the detachment of the cells can be investigated at the pre-defined observation window in real time. The exact solution for the velocity field was validated by comparing the analytical velocity profile with those obtained from both numerical simulation and experimental particle image velocimetry. The parabolic WSS gradient can be generated stably and consistently over time at a steady-state condition and easily modulated by changing the flow rate for the given ETRIC geometry. The WSS gradient in the ETRIC is in a symmetric parabolic form, and this symmetry feature doubles the experimental data, thereby efficiently minimizing the number of experiments. Finally, a WSS gradient ranging from 0 to 160 dyn/cm^2 was generated through the present ETRIC, which enables not only to measure the adhesion strength but also to investigate the time-dependent detachment of NIH-3T3 cells attached on the glass. *Published by AIP Publishing*. [http://dx.doi.org/10.1063/1.4965822]

I. INTRODUCTION

Cell adhesion is a primary and crucial process in cell growth, including attachment, migration, proliferation, and differentiation, because it mediates cellular response through the integrin binding between the cell and the substrate to which the cell adheres.[1] Cell adhesion strength is a good measure for evaluating cell adhesion, and it can be examined by measuring the detachment force of cells by using controllable forces. The cell adhesion strength has been quantified into two different physical quantities; (1) normal adhesion force (force term, N or dyn) and (2) shear adhesion strength (shear stress term, Pa or dyn/cm^2).

A normal adhesion force was measured by applying normal force using a pipette tip,[2] an atomic force microscope (AFM) probe,[3] and through centrifugation.[4,5] The methods using a pipette tip or an AFM probe can directly measure the individual cell adhesion with high resolution of forces but have a low throughput since they deal with a single cell per measurement. The alternative methods applying normal force based on centrifugation have also been employed, since the high throughput is required to get statistically meaningful data in short time. They can deal with a number of cells per measurement; however, these methods cannot generate enough force to detach cells due to safety issue of the centrifuge equipment.

[a)]Author to whom correspondence should be addressed. Electronic mail: smkds@postech.ac.kr. Telephone: +82 54-279-2183. Fax: +82 54-279-5912

On the other hand, the shear adhesion strength was measured by applying hydrodynamic wall shear stress (WSS). It is a promising method for high-throughput measurements with the capability of applying the enough force to detach cells. Various methods to generate WSS have been suggested to measure cell adhesion strength; these methods include the use of a parallel-plate chamber,[6–10] a spinning disk,[11,12] and a tapered microfluidic channel.[13,14] A parallel-plate chamber is a simple system used to generate a single WSS level between two plates with a controllable gap at a given flow rate. Because of its simple system setup and for the optical advantage, it is widely used for the cell adhesion measurement including time-dependent behaviors. Even though the number of experiments is reduced by applying the identical WSS level to the population of adhered cells, a number of experiments are still required to determine the adhesion strength of cells in response to different WSS levels. So, multiple experiments should be conducted for the cell adhesion measurement with the parallel-plate chamber with different flow rates. To minimize the multiple experiments to reduce laborious work, using a spinning disk and a tapered microfluidic channel as alternatives has been suggested by generating a WSS gradient under given experimental conditions. The spinning disk generates a WSS gradient along the radial direction by rotating the disk where cells are attached to the substrate in a massive liquid reservoir. The attached cells are exposed to the different levels of WSS drawn from the relative motion of the disk with respect to the surrounding stationary liquid as the disk rotates. The WSS level is linearly proportional to the radial distance from the center of the rotation axis and can be easily controlled by its rotation speed; thus, the cell detachment can be observed on a large range of WSS gradient at once. However, due to the movement of the disk that cells adhered, the disk cannot offer real-time observation of cell detachment. The tapered microfluidic channel generates a WSS gradient with varying channel widths along the flow direction. The velocity of the fluid increases with decreasing channel width to maintain mass conservation; therefore, the WSS increases with decreasing channel width at a given flow rate. The adhesion strength can be evaluated with the tapered channel through identifying a detachment region by moving the observation window along the flow direction, which means that the tapered channel cannot offer real-time observation of cell detachment. In this regard, there is still a strong demand for the development of a cell adhesion assay platform that provides (1) a WSS gradient within pre-defined observation window at a given flow rate and (2) a stable and consistent WSS gradient over time to measure the cell adhesion strength efficiently in real time with a minimum number of experiments.

In this paper, we present the equilateral triangular channel (ETRIC), a novel microfluidic channel that has an equilateral triangular cross-section. The ETRIC can apply a WSS gradient perpendicular to the flow direction stably and consistently with a single flow rate, and the *in situ* cell detachment within the pre-defined observation window can be investigated. Notably, the ETRIC has an exact analytical solution for the velocity field that was validated by both numerical and experimental methods, which exists in the entire channel region of the ETRIC. Thus, the WSS gradient at the bottom surface can be easily predicted and modulated. Also, the WSS gradient is in a symmetric parabolic form in the perpendicular direction of the flow, so that the experimental data can be doubled with a single experiment because of the symmetry; thus, the cell adhesion strength can be measured with a minimum effort. Moreover, due to that the simple design of the ETRIC only requires a straight channel, the observation setup does not need to move for screening of the cell detachment. Therefore, it is adaptable for investigating the *in situ* time-dependent detachment behavior of cells in real time. The adhesion strength and time-dependent detachment behavior of NIH-3T3 cells on the glass substrate were successfully evaluated using the ETRIC.

II. THEORY AND DESIGN

The schematic approach for conducting cell adhesion assay using the ETRIC is shown in Fig. 1(a). The equilateral triangular cross-section of the ETRIC generates a non-uniform velocity field at the bottom surface where maximum and minimum velocities are developed at the center and both side regions, respectively, thereby inducing a WSS gradient at the bottom

surface across the cross-section. When the flow is introduced into the ETRIC, the WSS gradient, which is in the form of parabolic shape illustrated as a blue line in Fig. 1(a), is gradually generated along the channel at a given flow rate. After exposure of the WSS gradient to the adhered cells, the cells would be detached in response to different levels of WSS. Most of the cells would be detached in the high shear region, illustrated as a red zone in the center region (Fig. 1(a), bottom); the others would remain adhered to the substrate in the low shear regions in both side regions of the bottom surface. The cell adhesion strength can be measured by screening the corresponding WSS of the detached cells.

The exact solution for the velocity field of the flow in ETRIC can be derived from the Navier–Stokes equation, assuming a Poiseuille flow: pressure driven, steady-state flow of a liquid through a long, straight, and rigid channel. Only an analytical exact solution for the velocity field of the Poiseuille flow in the channel with an equilateral triangular cross-section exists among those with general triangular cross-sections or any other rectangular cross-sections. Only a z-directional velocity field depending on x- and y-coordinates exists because of the translational invariance of the ETRIC along the channel direction in the z-axis of Fig. 1(a). The Navier–Stokes equation then becomes[15]

$$\left[\frac{\partial^2}{\partial x^2}+\frac{\partial^2}{\partial y^2}\right]v_z(x,y)=-\frac{\Delta p}{\mu L}, \tag{1}$$

where v_z is the z-directional velocity of the flow, Δp is the pressure drop, L is the channel length, and μ is the dynamic viscosity of the fluid, with a boundary condition of $v_z = 0$ on the wall.

The expression of the boundary of the ETRIC cross-section for the given coordinate system, as shown in Fig. S1, can be used as a trial solution for the velocity field, which naturally satisfies the no-slip boundary condition of $v_z(x,y)=v_0 y\left(y-\sqrt{3}x-\frac{\sqrt{3}}{2}a\right)\left(y+\sqrt{3}x-\frac{\sqrt{3}}{2}a\right)$, where a is the channel size (a length of each side of the equilateral triangle) and v_0 is a constant calculated as $v_0=\frac{1}{2\sqrt{3}}\frac{\Delta p}{a\eta L}$. Since the volumetric flow rate Q can be calculated from the integration of velocity field over the cross-section, $\mathrm{Q}=\int\int v_z(x,y)\,\mathrm{dx}\,\mathrm{dy}=\frac{3}{160}v_0a^5=\frac{\sqrt{3}}{320}\frac{a^4}{\eta L}\Delta p$. Hence, the exact form of the velocity field becomes

$$v_z(x,y)=\frac{160}{3}\frac{Q}{a^5}y\left(y-\sqrt{3}x-\frac{\sqrt{3}}{2}a\right)\left(y+\sqrt{3}x-\frac{\sqrt{3}}{2}a\right). \tag{2}$$

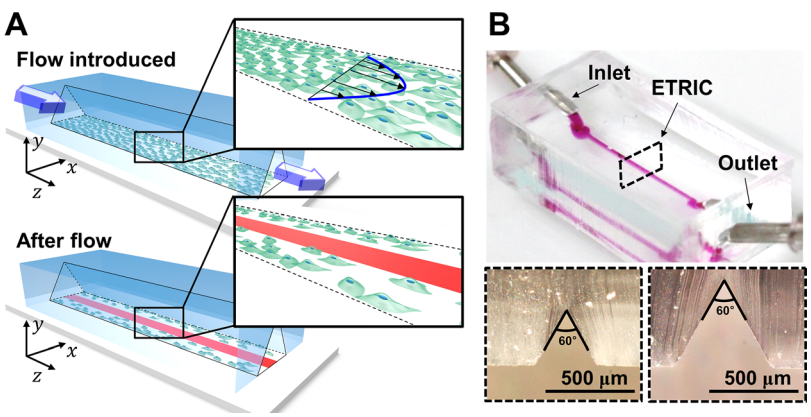

FIG. 1. (a) Schematic diagram of the cell adhesion assay with the equilateral triangular channel (ETRIC). When flow is introduced into the adhered cells, a parabolic wall shear stress (WSS) gradient is applied to the adhered cells. (Top) After introduction of the flow, the cells exposed to the high WSS, center region illustrated with the red region, would be detached, while the cells exposed to the low WSS would be remained. (b) Overview of the fabricated ETRIC and cross-sectional view having different sizes of 350 and 550 μm. Both channels have the apex angle of 60° showing the equilateral triangle cross-section.

Then, the WSS, τ_{wall} at the bottom surface can be expressed in a simple form as

$$\tau_{wall} = 40\frac{\mu}{a^3}Q\left(1 - 4\left(\frac{x}{a}\right)^2\right). \tag{3}$$

Notably, (1) the WSS gradient is stably and consistently induced in the ETRIC over time at a steady-state condition; (2) the induced WSS gradient has a symmetric parabolic form in the x-direction, i.e., perpendicular to the flow direction; and (3) the maximum WSS is proportional to the flow rate, viscosity of the fluid, and inverse of the third power of channel size. The maximum WSS can be designed by the channel size in consideration of the cell adhesion assay of interest because of the sensitive dependence of WSS on channel size (i.e., inverse third power). At a given channel size, the parabolic WSS gradient can be easily modulated by changing the flow rates through a syringe pump or the fluid itself to change the viscosity. For example, to apply the physiological shear stress range *in vivo* (0–20 dyn/cm^2) on the suggested ETRIC, the flow rate of 0.5 ml/min satisfies the desired shear stress range in the channel with the size of 550 μm. In this paper, to induce detachment of the adhered cells, we applied maximum 6 ml/min of flow rate, corresponding to 0–240 dyn/cm^2 of shear stress.

Due to the assumption of Poiseuille flow, a laminar flow condition and an entrance length should be considered when designing the microfluidic channel. For the laminar flow condition, the Reynolds number (Re) should be less than 2300 ($Re < 2300$). Since the Re depends on the viscosity, density, average velocity of the fluid, and characteristic lengths of the channel geometry, the maximum flow rate can be determined at a given channel size for the laminar flow condition. For the channel size of $a = 550\,\mu$m, a hydraulic diameter D_H is calculated as $\frac{a}{\sqrt{3}} = 317\,\mu$m. The maximum flow rate, for which the flow can be considered as laminar flow, is 55 ml/min (maximum shear stress of 2200 dyn/cm^2). We used the flow rates of 2, 3, 4, 5, and 6 ml/min for the channel size of 550 μm, and for all cases, the flow can be considered as laminar. Additional advantage of the laminar flow is that the roughness (generated during fabrication of the channel) has no discernible effect on the flow according to the Moody's chart. The entrance length is also important to expect the fully developed flow. Since the entrance length is related to the Re, it changes when the flow rate changes; higher flow rate needs longer entrance length. For the extreme case (flow rate of 6 ml/min at the 550-μm ETRIC), the entrance length was calculated as $l_{ent} \sim 0.05 \cdot Re \cdot D_H = 3.83$ mm. Since we used a microfluidic channel having the length of 20 mm and observed cells in the middle region (10 mm from the entrance), the flow is assumed to be fully developed.

III. EXPERIMENTAL METHODS

A. Fabrication of ETRIC

The ETRIC was fabricated through polydimethylsiloxane (PDMS) replica molding based on a micromachining process (Fig. 2). A master template with a protruded relief for the ETRIC was achieved by following a two-step micromachining process with a micromilling machine (EGX-350, Roland). A standard end mill was used for the first machining process to fabricate a protruded microchannel having a rectangular cross-section (Fig. 2(a)). A 60° tapered end mill was used for the second step of the micromachining process to cut the edge of the rectangular microchannel and obtained a protruded equilateral triangular shape with a precisely controlled milling path (Fig. 2(b)). A PDMS prepolymer mixture (Sylgard-184; Dow Corning, a 10:1 weight ratio of base to curing agent) was poured onto the master template and then vacuumed to remove residual bubbles. PDMS was then cured in a 65 °C oven for 4 h (Figs. 2(c) and 2(d)). A PDMS ETRIC was treated with oxygen plasma to prevent bubble formation while loading the liquid into the channel. The bottom surface of the PDMS ETRIC was relatively rough due to the replication of the tool path on the master template so that it was coated with the PDMS prepolymer mixture before bonding with a glass slide. The PDMS ETRIC on the glass slide was baked again inside the 65 °C oven for 4 h for bonding

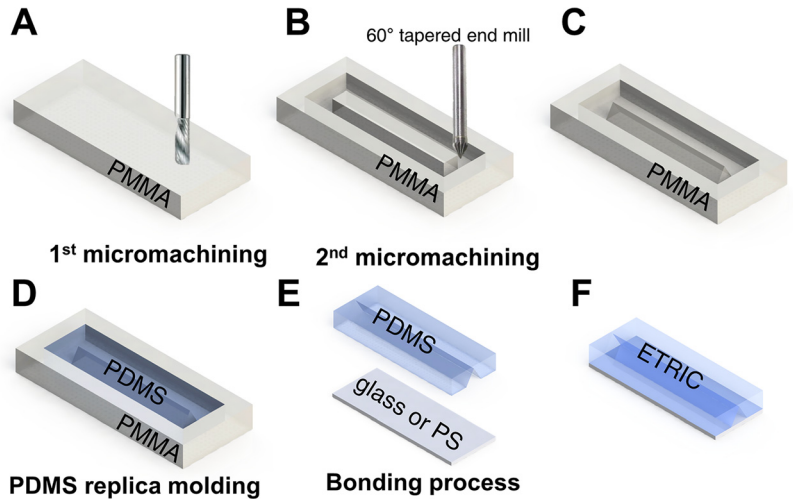

FIG. 2. Schematic for the fabrication of equilateral triangular channel (ETRIC). (a)–(c) Two-step micromachining to fabricate the master mold with a standard end mill and a 60° tapered end mill with a precisely controlled milling path. (d) PDMS replica molding to replicate the PDMS ETRIC. (e) Bonding process of the PDMS ETRIC to the glass substrate. (f) Fabricated ETRIC on the glass substrate

(Figs. 2(e) and 2(f)). Cross-sectional views of the fabricated ETRIC are shown in Fig. 1(b). The channel has an apex angle of 60° with an equilateral triangular cross-section. The roughness generated from the micromilling process was less than 1 μm, which is small enough compared to the channel size of 550 μm (Fig. S2).

B. Particle image velocimetry (PIV) analysis

A suspension of 5 μm-diameter polystyrene fluorescent particles (Thermo Scientific Corp. and Invitrogen) was diluted with deionized water to achieve 1% concentration (w/v). The ETRIC was coated with bovine serum albumin to prevent the adhesion of particles inside the channel walls. The ETRIC was then placed on the inverted fluorescence microscope (Axovert 200, Carl Zeiss). The focal plane was set at 30 μm above the glass slide to ensure a sufficiently developed velocity for observation because the flow velocity near the glass slide is almost zero due to the no-slip condition. Two sizes of ETRIC ($a = 350$ and 550 μm) were prepared, and different flow rates ($Q = 3$ and 5 μl/h) were applied for both channels. A total of 100 images were taken in one set of the experiment with the time interval of 0.5 s.

After acquiring the sets of images, the velocity of the particles was analyzed through MATLAB using the open-source software OpenPIV (www.openpiv.net). For analysis, a 16 × 16 pixel area was used for both the interrogation window and the spacing overlap, with S/N type 2, outlier filter = 100, and jump = 1. The 99 velocity data sheets were extracted from one set of 100 images by comparing the two image sequences. The velocities of the particles at the same streamline were assumed to be the same and were averaged by combining all of the 99 data sheets. The representative particle image sequence and the image showing the calculated velocity from two image sequences are shown in Fig. S3.

C. Numerical simulation

Finite element simulations through COMSOL multiphysics (COMSOL, Inc., USA) were conducted to calculate the velocity profiles inside the ETRIC for comparison with the analytical velocity profiles. The 3D geometry of the ETRIC was chosen as a computational domain under laminar and steady-state flow conditions. The ETRIC was designed to have two sizes of 350 and 550 μm and a channel length of 20 mm, similar to that used in the PIV analysis. The applied volume flow rates were set as 3 and 5 μl/h; hence, four simulations were conducted

with different channel sizes and flow rates. Deionized water was chosen as a working fluid, with a density of 1000 kg/m3 and a dynamic viscosity of 1 mPa s; hence, all conditions were the same as those in the PIV analysis. The volume elements for ETRIC were densely distributed near the bottom surface where the actual WSS was applied to the cells.

D. Cell adhesion assay

The fabricated 550 μm-ETRICs were washed with 70% ethanol (Merk) and then with deionized water before introducing the flow. The whole device was carefully filled with a sterile phosphate buffered saline (PBS) solution to remove the remaining bubbles in the channel.

NIH-3T3 cells were cultured in Dulbecco's modified Eagle's medium (Hyclone) supplied with 10% fetal bovine serum (Hyclone) and 1% penicillin-streptomycin (Gibco) in a humidified incubator at 37 °C with 5% CO_2. After being rinsed with sterile PBS solution, cells at a density of 1.5×10^6 cells/ml were stained with 4 μM Calcein AM (Life Technologies) for the fluorescence of live cells and then seeded to the ETRICs by delicate pipetting. Two different levels of cell adhesion strengths were evaluated by changing cell adhesion time of 2 and 6 h whose values correspond to early adhesion and full adhesion times, respectively.[18,19] After 2 h and 6 h of cell incubation, the culture medium (also PBS can be used, which shows almost similar results at 2 h of adhesion; Fig. S4) was introduced into the ETRIC by a syringe pump (KDS230, KD Scientific) at a flow rate of 0.01 ml/min, inducing the maximum WSS of 0.4 dyn/cm^2, to remove non-adherent cells. The culture medium was then applied to the ETRICs at different flow rates of 2, 3, and 4 ml/min to the 2 h incubated cells, and 4, 5, 6 ml/min to the 6 h incubated cells. For the flow rates of 2, 3, 4, 5 and 6 ml/min, the corresponding WSS ranges were 0–80, 0–120, 0–160, 0–200, 0–240 dyn/cm^2, respectively. Each experiment was carried out in triplicate.

E. Observation setup for adhesion assay and data analysis

Due to the inclined wall of the ETRIC, there is black shadow in the center region of the ETRIC with the phase contrast imaging, which is commonly used for cell observation. To neglect such an effect, a custom-built fluorescence observation system was used to investigate the cell detachment behaviors in the ETRIC. The ETRIC was placed on the transparent mounting plate positioned on a digital camera (EOS-650D, Canon) pointing upward. Green cellophane was fixed in front of the camera lens to serve as the filter that blocks all light waves, except for green. Live fluorescent cells were exposed to blue light at 495 nm, so that the remaining adhered cells would emit green light. The camera was set at a continuous shooting mode with a time interval of 1 s for 2 min to measure the cell adhesion strength and video recording mode for investigating the time-dependent detachment with a recording time of 2 min.

The sets of images were color-adjusted to distinguish the cells from the background through the image analysis program NIH ImageJ (https://imagej.nih.gov/ij/). The adjusted parameters included contrast, image brightness, intensity threshold, cell area, and cell circularity. The position data of every cell were automatically measured using the program. The number of cells in the region of interest can then be acquired by counting from the position information. The adhered cell fraction (ACF) was calculated and plotted with respect to the WSS level because the level of WSS varies spatially in perpendicular to the flow direction. The image set of the color-adjusting process and the position data measuring image are shown in Fig. S5.

IV. RESULTS AND DISCUSSION

A. Flow characteristics in the ETRIC

We compared the analytical velocity profile with those obtained from the numerical simulation and PIV analysis to validate the analytical solution for the velocity field in the ETRIC in Eq. (2). Fig. 3 plots three velocity profiles from the analytical solution, numerical simulation, and PIV analysis at the plane 30 μm above the bottom surface of the ETRIC, as schematically shown in Fig. S6. The velocity profiles of the analytical solution and the numerical simulation exactly coincided with each other for all cases. The experimental velocity profiles fitted well

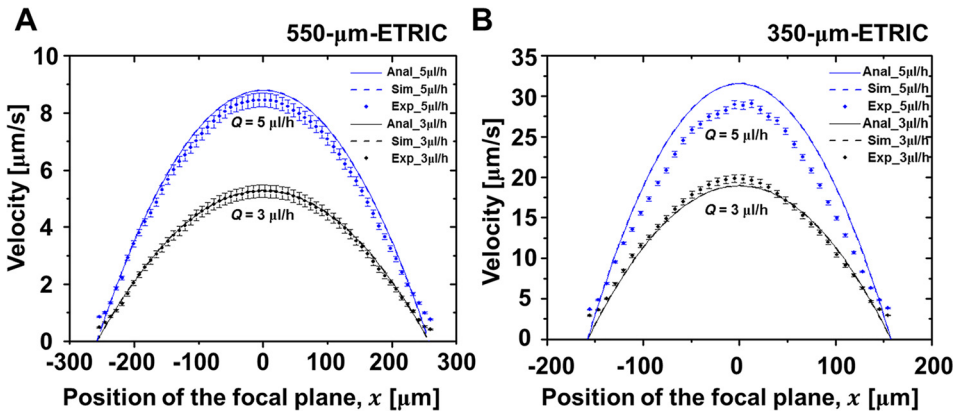

FIG. 3. Velocity profiles at the 30 μm above the bottom surface comparing analytical solution (Anal), numerical simulation (Sim), and experimental measurements through PIV analysis (Exp) when applied different flow rates of 3 and 5 μl/h in different sizes of channels (a) for the 550-μm-ETRIC and (b) for the 350-μm-ETRIC. The analytical solution, numerical simulation, and experimental measurements were well matched for all cases except for the case of channel size of 350 μm with a flow rate of 5 μl/h.

with the analytical and numerical ones, except for the case when the channel size was 350 μm at the flow rate of 5 μl/h. In this case, a lower PIV velocity profile was measured compared with the analytical and numerical ones because of the limitation of the current PIV system setup in which the movement of the particles having a certain high velocity cannot be captured. The results indicated that the analytical exact solution for the velocity profile of the Poiseuille flow in the ETRIC given in Eq. (2) is valid under the steady-state condition, which is applicable for the prediction or design of the velocity field under real experimental conditions.

WSS is the actual force that is directly applied to the adhered cells. Given its close relation to the velocity gradient of the fluid at the bottom surface, the WSS can be indirectly calculated using the information on velocity field and fluid properties. The measured velocity profile matched both the analytical and numerical velocity profiles; thus, the induced WSS in the ETRIC calculated from Eq. (3) was considered valid, although the WSS cannot be directly measured at the bottom surface. This aspect is a huge advantage of the ETRIC for carrying out cell adhesion assay because numerical simulations are not required to calculate the WSS at the given geometry of the ETRIC, fluid properties, and flow rate.

B. Measuring cell adhesion strength

The cell adhesion strength of the NIH-3T3 cells attached on the glass substrate was measured by comparing the numbers of adhered cells before and after exposure to the WSS gradient for 2 min. The adhered cell fraction (ACF) was determined as a ratio of the number of cells after exposure to WSS to the number of cells before exposure

$$\text{adhered cell fraction (ACF)} = \frac{\text{number of cells after exposure to WSS}}{\text{number of cells before exposure to WSS}},$$

where the ACF varies from zero to unity: ACF = 0 when all of the cells are detached and ACF = 1 when all of the cells are remained adhered to the substrate.

The ACF was evaluated with the 550 μm-ETRIC at flow rates of 2, 3, and 4 ml/min for 2 h incubated cells, and 4, 5, and 6 ml/min for 6 h incubated cells. For the flow rates of 2, 3, 4, 5, and 6 ml/min, the corresponding WSS ranges were 0–80, 0–120, 0–160, 0–200, and 0–240 dyn/cm^2, respectively. Fig. S7 shows the representative images of live fluorescent cells attached on the bottom surface of the ETRIC before and after exposure to the WSS in the pre-defined observation window. Proper sectioning of the channel area in perpendicular to the flow direction in the observation window is required to evaluate the ACF and cell adhesion strength due to the WSS variation. Interestingly, there is a conflict between acquiring the high accuracy of

TABLE I. Wall shear stress range with different applied flow rates in the different sectioned position ranges and center positions in the 550 μm-ETRIC.

				Shear stress level (dyn/cm^2)		
	Section #	Position (μm)	Position range (μm)	2 ml/min	3 ml/min	4 ml/min
	S1	0	−25 ∼ 25	79.81 ± 0.33	119.72 ± 0.50	159.62 ± 0.66
	S2	−50, 50	±25 ∼ 75	76.83 ± 2.65	115.25 ± 3.98	153.66 ± 5.30
	S3	−100, 100	±75 ∼ 125	68.88 ± 5.3	103.32 ± 7.95	137.76 ± 10.60
	S4	−150, 150	±125 ∼ 175	55.64 ± 7.95	83.45 ± 11.92	111.27 ± 15.90
	S5	−200, 200	±175 ∼ 225	37.09 ± 10.60	55.64 ± 15.90	74.18 ± 21.19

the calculated ACF and increasing the screening resolution of adhesion strength (i.e., WSS level of detaching cells). To obtain the high accuracy of ACF, a sufficient population of cells is needed in the observation region; meanwhile, the high screening resolution requires fine sectioning of the channel area to have a narrow range of WSS variation. Statistically, 30 samples are usually regarded as a minimum number to have sufficient accuracy.[16] For the 550 μm-ETRIC, the sectioning width of 50 μm results in an average over 50 cells/sectioned region. In this regard, we divided the channel area in the observation window into nine sections with a 50 μm width in perpendicular to the flow direction (i.e., along the direction of the WSS gradient, Fig. S8) to obtain a statistically significant number of cells. We did not consider the two outmost side sections when investigating the cell adhesion because of less adhered cells without loss of generality and unexpected WSS level due to the confinement effect, where the channel heights are as small as cell size.[9,26] Excluding the outmost side sections, there exist two sections that had an identical WSS level because of the symmetric WSS gradient, and they were indicated as the same section region number, i.e., S2–S5 except for the center section (S1), as indicated in Fig. S8. The position and WSS level of each section are listed in Table I. We counted the numbers of live fluorescent cells before and after exposure to the WSS in the captured images and then calculated the ACF. The representative ACFs from the 550 μm-ETRIC at a flow rate of 4 ml/min on 2 h incubated cells, which corresponded to the WSS gradient range of 0–160 dyn/cm^2 with respect to the section region, are plotted in Fig. 4(a). The calculated ACF was plotted at the center position of the corresponding section on the abscissa as red open dots with bars (left ordinate). The WSS distribution, which was determined from Eq. (3), was plotted with a blue dotted line (right ordinate). Fig. 4(a) shows that the ACF exhibits an inverse

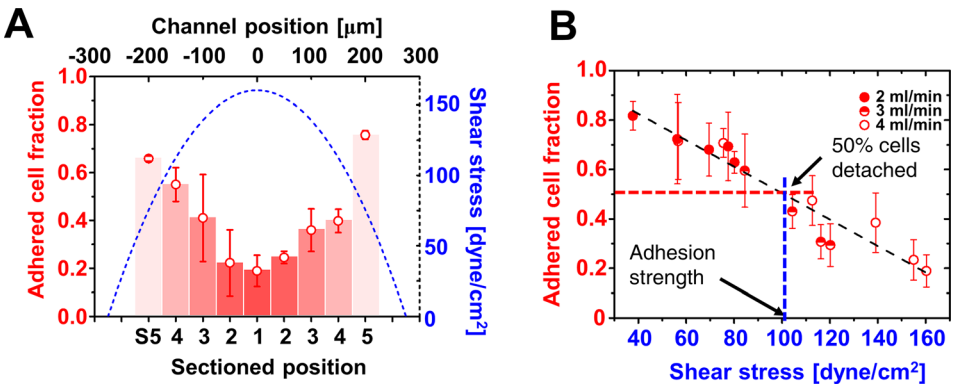

FIG. 4. (a) Adhered cell fraction (ACF) plotted with respect to the channel position with red dots and wall shear stress (WSS) distribution was plotted with blue dotted line when the 4 ml/min of flow was applied to the 2 h incubated cells. The colored bar indicates the sectioned channel position. (b) Reconfiguration of ACF with respect to the WSS. The cells tend to detach in the high WSS region with the critical adhesion strength of 104.41 and 125.01 dyn/cm^2 for 2 h and 6 h adhesion, respectively.

shape of the applied WSS gradient. The lowest ACF was obtained at the highest WSS in S1, whereas the highest ACF was observed at the lowest WSS in S5.

The measured ACFs with respect to the WSS in the ETRIC for 2 h and 6 h incubated cells are shown in Fig. 4(b). The symmetric feature of the WSS gradient doubled the data counting cells with a single experiment, which obtained a more reliable ACF result with the ETRIC. The measured ACF decreased almost linearly with increasing exposed WSS level, thereby enabling us to rationally determine the cell adhesion strength with the ETRIC. We used a critical adhesion strength to quantify the cell adhesion strength, a WSS level where 50% of the cells were detached after exposure to the flow as an adhesion indicator, which was generally suggested in previous studies.[11,13,17] Fig. 4(b) shows that the critical adhesion strength of the NIH-3T3 cells on the glass substrate is approximately 104.41 ± 12.10 and $125.01 \pm 23.00\,\text{dyn/cm}^2$ (standard error was calculated from the linear fitting) after 2 h and 6 h of adhesion, respectively. For NIH-3T3 cells, cells fully adhered at 6 h of adhesion.[18] The critical adhesion strength at 6 h of adhesion was 20% higher than at 2 h of adhesion, indicating that the cell adhesion process was advanced until 6 h. The critical adhesion strength at 2 h of adhesion was compared to the previously reported one. Truskey *et al*. reported that the statistic log-normal distribution of NIH-3T3 cells on glass has an average value of $82.4\,\text{dyn/cm}^2$ with a standard deviation of $108.1\,\text{dyn/cm}^2$ under the 2 h of cell adhesion on the bare glass substrate, as our experiment (such a large standard deviation is typical of a log-normal distribution and indicates data skewness).[19,20] They used the parallel-plate chamber to measure the cell adhesion strength, and nine experiments were conducted to acquire nine ACF measurements. In the present study, we only carried out the cell adhesion assay in the ETRIC in triplicate at three flow rates (total nine experiments) with nine sections, resulting in a total of 81 ACF measurements. Such a large number of ACF measurements enables us to obtain a more accurate and precise measurement with a narrower range of cell adhesion strength than the value suggested by Truskey *et al*. with the same number of experiments.

As mentioned in the introduction, the cell adhesion strength has been quantified based on the normal adhesion force, and the shear adhesion strength, respectively. In a recent work by Cho *et al*., there are no exact correlations between the normal adhesion force and the shear adhesion strength, but it has been elucidated that the required activation energy to peeling-off detachment of particles through applying shear stress is small compared to the energy to normal lift-off detachment.[21] Although there remains whether the normal adhesion force or shear adhesion strength is a suitable parameter for quantification of the cell adhesion, the cell adhesion strength with the shear stress term has been widely reported with the various cell types on the different substrates.[6–14,22,23] Besides, there have been attempts to demonstrate the mechanical model to estimate the magnitude of the normal force when the WSS is applied to the adhered cells to evaluate the binding force of the integrin receptors to extracellular ligands.[12,24–26] Hammer *et al*. suggested a simple mechanical model to estimate the normal adhesion force from the cell adhesion strength measured by the shear stress term.[24] Gallent *et al*. improved the mechanical model by applying a peeling-off detachment model to calculate a detachment peeling force when the shear stress is exerted on the adhered cells.[12] According to the shear-detachment model from Gallent *et al*., with the assumptions of the cells having a spherical shape with the radius $\boldsymbol{R}$, adhere to the area having the radius $\boldsymbol{a}$, and with the applied external shear stress $\boldsymbol{\tau}$, the tensile force acting at the leading edge of peeling motion $\boldsymbol{F_T}$ can be expressed as,

$$\boldsymbol{F_T} = \boldsymbol{32R^2\tau}\sqrt{1+\left(\frac{\boldsymbol{0.8R}}{\boldsymbol{a}}\right)^2}. \tag{4}$$

In our observation with the critical adhesion strength of 104.41 and $125.01\,\text{dyn/cm}^2$, for 2 h and 6 h of adhesion, the NIH-3T3 cells on bare glass have a binding force of 24 nN and 28 nN, respectively, calculated from Eq. (4) assuming that the cells have the radius $\boldsymbol{R} = 7.5\,\mu\text{m}$ and are adhered on the circular area with the radius of $\boldsymbol{a} = 7.5\,\mu\text{m}$ (Data from the average diameter of

NIH-3T3 cells and observation, respectively). Gallant *et al*. measured the NIH-3T3 cells on the fibronectin (FN) coated surface, which have the binding force of 200 nN, which is an order of magnitude higher compared to cells on the bare glass in our experiments. This quantitative measurement coincides with the fact that the FN enhances the cell adhesion strength by providing more integrin binding sites.[27]

C. Time-dependent cell detachment kinetics

A time-dependent cell detachment behavior could be also observed *in situ* within a single observation window in the ETRIC at a given flow rate in real time (supplementary video, snapshots are shown in Fig. 5(a)). Different sections with a width of 78 μm (five sections excluding the outmost area, Fig. 5(a)) were applied to achieve about over 50 cells/sectioned region. The ACF was plotted with flow exposure time to show the time-dependent detachment behaviors of the 2 h incubated cells at three sections corresponding to three WSS levels at a flow rate of 3 ml/min, inducing the WSS gradient within the range of 0–120 dyn/cm^2 (Fig. 5(b)). Cell detachment exhibited three stages during the experiments. At the first stage, the initial detachment of the cells was observed within 20 s; about 10% and 30% of the cells were detached at the WSS levels of 78.5 and 119.0 dyn/cm^2, respectively. At the next stage, a stabilized adhesion behavior was observed, showing steady ACF values until 60 s. At the final stage, additional detachment was observed after 60 s. At 120 s, the ACF values were 0.7 and 0.45 at the WSS levels of 78.5 and 119.0 dyn/cm^2, respectively, consistent with the results from Fig. 4(b). The time-dependent detachment behaviors of the cells at the different flow rates of 2 and 4 ml/min corresponding to the WSS gradient ranges of 0–80 and 0–160 dyn/cm^2, respectively, are also additionally plotted in Fig. S9, showing a similar tendency to Fig. 5(b). Although the cells with identical cell type seeded and adhered to the substrate at the same time, cell detachment behaviors exhibited different characteristics of adhesion. The low-adhesion group of cells detached at the first stage within 20 s, whereas the high-adhesion group exhibited retarded detachment at the third stage after 60 s (Fig. 5(b)). These findings may take into account with the work done by Christ *et al*.[28] They observed the different cell detachment behavior with three distinct modes by changing their cytoskeleton formation. Most of the cells detach with a slight change in the cytoskeleton, but the other cells experience considerable deformation of shape or rupture, showing that the cells are heterogeneous even in the same cell populations.

We developed an *in situ* real-time observation system to detect cell detachment with respect to the WSS level and time simultaneously, and this technique can be applied in the adhesion-based cell separation.[29,30] Since the cell detachment is a cumulative phenomenon, the detachment is affected by both the WSS level and duration time. Kwon *et al*. suggested the

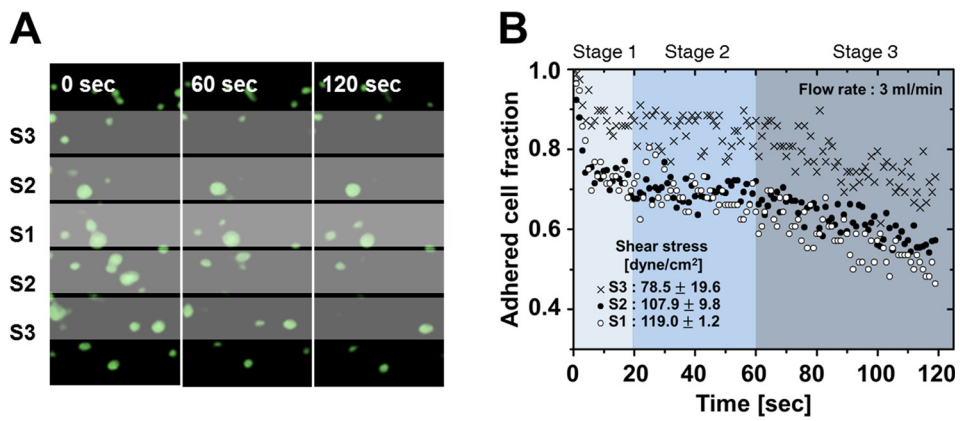

FIG. 5. (a) Snapshot at 0, 60, and 120 s after the flow was introduced, and 5 sectioned area for the analysis response to the different levels of WSS. (b) Adhered cell fraction with respect to time, in response to the different WSS levels at a flow rate of 3 ml/min. There exhibit 3 stages of detachment, initial detachment within 20 s, stable detachment region until 60 s, and additional detachment region after 60 s.

effective WSS level and duration time to separate cancer cells from the normal cells on different surface topography and adhesion times.[29] However, they conducted the discrete experiments on the parallel plate flow system with a few experimental conditions for the WSS level and time. To effectively separate distinct cell types based on the adhesion difference, cell detachment should be examined with a wide range of WSS with duration time for each cell. Through the ETRIC with the *in situ* real-time observation system, the cell detachment can be examined effectively by applying the WSS gradient for certain amount of time. After identifying the detachment behavior of individual cells, the sets of values (WSS level with duration time) can be presented to optimal separation based on the different detachment behavior, which will be our future work.

V. CONCLUSIONS

We proposed the ETRIC as a new microfluidic-based platform for *in situ* cellular adhesion assay. The ETRIC can generate a stable and consistent parabolic WSS gradient at a single flow rate, which can screen cell detachment in response to spatially different levels of WSS within an observation window in real time. A simple form of exact solution exists for velocity field and WSS distribution; therefore, the desired WSS levels can be easily designed and modulated. The symmetric parabolic form of the WSS gradient doubles the experimental data, thereby minimizing the number of experiments efficiently. A time-dependent cell detachment behavior can also be investigated with the ETRIC because it allows real-time observation. In this manner, the ETRIC can be used as a new screening platform for cell adhesion-based experiments and can be further extended to evaluate the cell adhesion strength in response to various *in vitro* cell microenvironments.

SUPPLEMENTARY MATERIAL

See supplementary material for the schematic showing the cross-section of the equilateral triangular channel (ETRIC) with the x-and y- coordinates, and the equations for boundaries (Fig. S1), SEM images of the ETRIC surface (Fig. S2), images of movement of particles for particle image velocimetry (Fig. S3), adhered cell fraction with respect to shear stress, conducted with PBS and culture medium (Fig. S4), image set showing the color-adjusting process to measure the position of the cells (Fig. S5), schematic showing the position of the focal plane (Fig. S6), representative images of live fluorescent cells before and after exposure to wall shear stress (Fig. S7), color-adjusted and cropped image to indicate the sectioned region and adhered cells before and after exposure to wall shear stress (Fig. S8), Time-dependent detachment behaviors of cells at different flow rates (Fig. S9), and representative video showing the detachment of the cells through real time observation for 2 min (supplementary movie S1).

ACKNOWLEDGMENTS

This work was supported by the National Research Foundation of Korea (NRF) grant funded by the Korea government (MSIP) (2014R1A2A1A01006527, 2011-0030075).

[1]R. O. Hynes, Cell **69**(1), 11–25 (1992).
[2]A. Tözeren, K. L. Sung, L. A. Sung, M. L. Dustin, P. Y. Chan, T. A. Springer, and S. Chien, J. Cell Biol. **116**(4), 997–1006 (1992).
[3]R. Merkel, P. Nassoy, A. Leung, K. Ritchie, and E. Evans, Nature **397**(6714), 50–53 (1999).
[4]D. R. McClay, G. M. Wessel, and R. B. Marchase, Proc. Natl. Acad. Sci. U.S.A. **78**(8), 4975–4979 (1981).
[5]L. Chu, L. A. Tempelman, C. Miller, and D. A. Hammer, AIChE J. **40**(4), 692–703 (1994).
[6]T. G. V. Kooten, J. M. Schakenraad, H. C. V. Mei, and H. J. Busscher, J. Biomed. Mater. Res. **26**(6), 725–738 (1992).
[7]H. Lu, L. Y. Koo, W. M. Wang, D. A. Lauffenburger, L. G. Griffith, and K. F. Jensen, Anal. Chem. **76**(18), 5257–5264 (2004).
[8]E. W. K. Young, A. R. Wheeler, and C. A. Simmons, Lab Chip **7**(12), 1759–1766 (2007).
[9]C. Couzon, A. Duperray, and C. Verdier, Eur. Biophys. J. **38**(8), 1035–1047 (2009).
[10]C. Verdier, C. Couzon, A. Duperray, and P. Singh, J. Math. Biol. **58**, 235–259 (2009).
[11]A. J. Garcia, P. Ducheyne, and D. Boettiger, Biomaterials **18**(16), 1091–1098 (1997).
[12]N. D. Gallant, K. E. Michael, and A. J. Garcia, Mol. Biol. Cell **16**(9), 4329–4340 (2005).

[13]P. Rupprecht, L. Gole, J.-P. Rieu, C. Vezy, R. Ferrigno, H. C. Mertani, and C. Riviere, Biomicrofluidics **6**(1), 014107 (2012).
[14]E. Gutierrez and A. Groisman, Anal. Chem. **79**(6), 2249–2258 (2007).
[15]H. Bruus, *Theoretical Microfluidics*, 3rd ed. (Oxford University Press, New York, 2008).
[16]R. V. Hogg and E. A. Tanis, *Probability and Statistical Inference*, 7th ed. (Prentice Hall, New Jersey, 2005).
[17]A. Rezania, C. H. Thomas, and K. E. Healy, Ann. Biomed. Eng. **25**(1), 190–203 (1997).
[18]S. Schile, M. Gruene, H. Dittmar, and B. N. Chichkov, Tissue Eng. C **18**(9), 688–697(2012).
[19]G. A. Truskey and J. S. Pirone, J. Biomed. Mater. Res. **24**(10), 1333–1353 (1990).
[20]S. C. Choi, *Introductory Applied Statistics in Science* (Prentice Hall, New Jersey, 1978).
[21]K. L. Cho, A. Rosenhahn, R. Thelen, M. Grunze, M. Lobban, M. L. Karahka, and H. J. Kreuzer, Langmuir **31**(40), 11105–11112 (2015).
[22]A. S. Goldstein and P. A. DiMilla, J. Biomed. Mater. Res. **59**(4), 665–675 (2002).
[23]A. J. Engler, M. Chan, D. Boettiger, and J. E. Schwarzbauer, J. Cell Sci. **122**(10), 1647–1653 (2009).
[24]D. A. Hammer and D. A. Lauffenhurger, Biophys. J. **52**(3), 475–487 (1987).
[25]G. A. Truskey and T. L. Proulx, Biomaterials **14**(4), 243–254 (1993).
[26]D. P. Gaver and S. M. Kute, Biophys. J. **75**(2), 721–733 (1998).
[27]S. Miyamoto, B.-Z. Kathz, R. M. Lafrenie, and K. M. Yamada, Ann. N. Y. Acad. Sci. **857**, 119–129 (1998).
[28]K. V. Christ, K. B. Williamson, K. S. Masters, and K. T. Turner, Biomed. Microdevices **12**(3), 443–455 (2010).
[29]K. W. Kwon, S. S. Choi, S. H. Lee, B. Kim, S. N. Lee, M. C. Park, P. Kim, S. Y. Hwang, and K. Y. Suh, Lab Chip **7**(11), 1461–1468 (2007).
[30]A. Singh, S. Suri, T. Lee, J. M. Chilton, M. T. Cooke, W. Chen, J. Fu, S. L. Stice, H. Lu, T. C. McDevitt, and A. J. Garcia, Nat. Methods **10**(5), 438–444 (2013).